



Topology Optimization and Additive Manufacturing of Customized Sports Item Considering Orthotropic Anisotropy

Jung-Hwan Park¹ · Bona Goo¹ · Keun Park¹

Received: 25 September 2018 / Revised: 19 March 2019 / Accepted: 23 May 2019 / Published online: 4 June 2019
© Korean Society for Precision Engineering 2019

Abstract

Topology optimization is a shape optimization method connected with finite element (FE) structural analysis, and has recently received increasing attention owing to rapid evolution of additive manufacturing (AM). In this study, a rifle support for the sport biathlon is developed by combining three-dimensional (3D) scanning, FE analysis, topology optimization, and AM. Considering that the biathlon requires a stable shooting motion under hard breathing after a distance of cross-country skiing, the rifle support was designed to be fitted to a human body based on 3D scanning data. Topology optimization was then performed to reduce the part weight efficiently, and its structural safety and stiffness were evaluated by FE analyses considering the orthotropic material properties and the relevant printing directions. The optimized design and printing direction were showed 12.7% improvements in the specific stiffness and 23–43% improvements in the structural safety according to the direction. The final design was fabricated using a fused deposition modeling type 3D printer with acrylonitrile butadiene styrene filament. Compression tests were then performed to evaluate its structural safety, and the resulting relative critical force showed a 40% improvement in comparison with the original design.

Keywords Topology optimization · Additive manufacturing · 3D printing · Finite element analysis · Customized sports item

List of Symbols

δ_{\max}	The maximum vertical displacement
F	Applied force
λ^*	Relative safety factor
V_0	Volume of the initial design
V	Volume of the modified design
k	Bending stiffness in the linear range
k^*	Relative bending stiffness
F_{crit}	Critical compressive force at failure
F^*	Relative critical force per unit mass
σ_{\max}	The maximum directional stress
σ_{allow}	The allowable stress

1 Introduction

Topology optimization is a method of structural shape optimization that determines the optimal structure in a design domain [1]. Through connection with structural finite element (FE) analysis, topology optimization is generally used to determine an efficient material distribution in a predefined domain so that the volume of the produced structure can be reduced while maintaining structural safety [2]. An efficient lightweight structure can thereby be obtained with minimal usage of material.

The topology optimization, however, has a drawback in that the optimized topology usually has a complicated shape and thus is costly in terms of manufacturing. In some cases, manufacturing has been nearly impossible using the traditional manufacturing technologies. In recent years, the rapid evolution of additive manufacturing (AM) has bridged the gap between topologically optimized design and the limitations restricting manufacturing [3]. More specifically, topologically optimized designs can be manufactured easily owing to the high design flexibility of AM. Various studies have utilized AM to manufacture topologically optimized designs with complicated shapes [4–7]. However, they

✉ Keun Park
kpark@seoultech.ac.kr

¹ Department of Mechanical System Design Engineering,
Seoul National University of Science and Technology, 232,
Gongneung-ro, Nowon-gu, Seoul 01811, Republic of Korea

performed topology optimization based on the isotropic assumption although most AM processes cause anisotropic material properties due to its layer-by-layer deposition [8, 9].

Another promising application area of AM is direct fabrication of customized or personalized products; biomedical applications such as bioimplants [10] or orthoses [11] are good examples of customization. Sports items are another application and they can enhance athletes' performance by customization [12]. Considering that biomedical or sports items are worn on the human body, they also require weight reduction and in this sense topology optimization may be a desirable approach.

In this study, a rifle support for biathlon is developed as a customized sports item. Biathlon is a winter sport that combines cross-country skiing with precision rifle shooting [13]. In biathlon, a stable shooting motion is essential even under hard breathing because athletes have to perform a series of shots after covering a distance of cross-country skiing [14]. To improve stability in the shooting motion, a rifle support is usually attached to the rifle butt in order to hold the rifle through contact with the athlete's shoulder. This study aims to further stabilize the athlete's shooting motion by customizing the rifle support to be fitted to a human body. For this purpose, the rifle support was initially designed based on three-dimensional (3D) scanning data.

To reduce the part weight with allowable structural safety and stiffness, topology optimization combined with finite element (FE) analysis was performed for design of the customized rifle support. Considering that the layered deposition of AM causes anisotropic mechanical properties, FE analyses and relevant topology optimization were performed based on orthotropic material properties. The effect of the printing direction and the relevant directional structural safety were also taken into account in the simulation. The optimal design candidate was then determined to have the highest specific stiffness and safety factor, and was then fabricated using a fused deposition modeling (FDM) type 3D printer. Experimental validations were also conducted to compare the structural safety of the optimally designed rifle support.

2 Design of a Customized Rifle Support

2.1 Design Overview

Figure 1a shows an image of a biathlon rifle with an attached shoulder support. It can be seen that the current support has a flat end, and cannot completely contact the human body. Although a curved rifle support can improve contact stability, a commercial product with a standard size and geometry cannot fit the human body, as shown in Fig. 1b. Such incomplete contact may result in unstable shooting motion, which

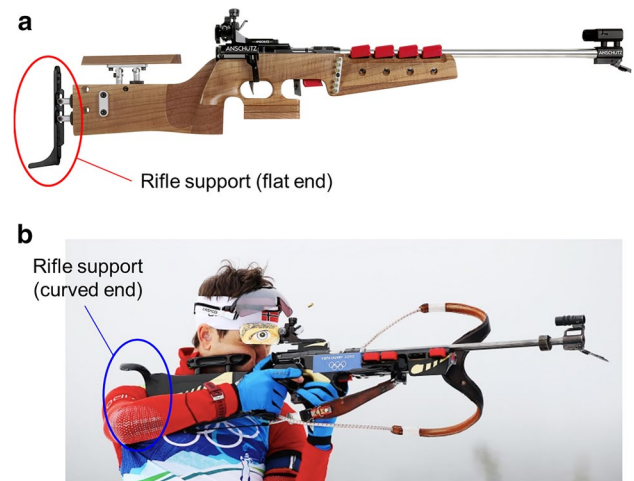


Fig. 1 Examples of rifle supports for biathlon: **a** flat shape, and **b** curved shape

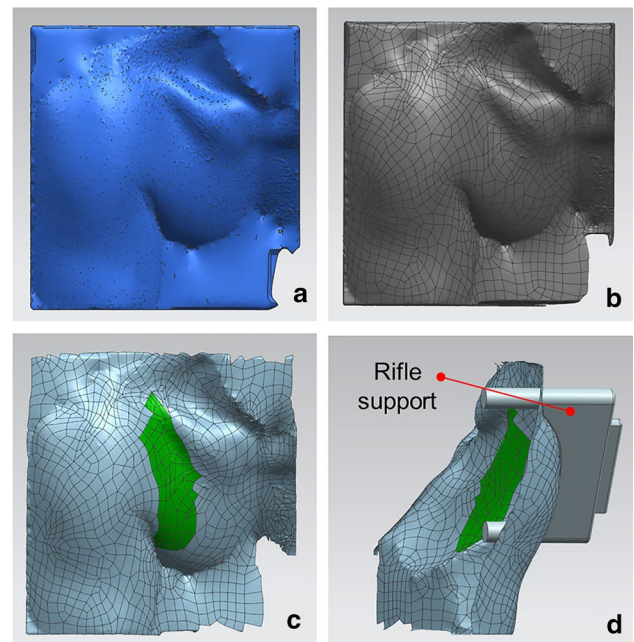


Fig. 2 Design procedure of a customized rifle support: **a** 3D scanned point cloud data, **b** generated surface data, **c** definition of the contact region, and **d** design of a rifle support

consequently deteriorates shooting performance. Thus, a customized rifle support is desirable to maintain complete contact with a human body.

To develop a customized rifle support, an athlete's shoulder was scanned while in the shooting position. A hand-held type 3D scanner (EinScan-Pro, SHINING 3D Technology GmbH, China) was used to obtain 3D point cloud data of the athlete's shoulder, as shown in Fig. 2a. These point cloud data were converted into 3D surface data, as shown

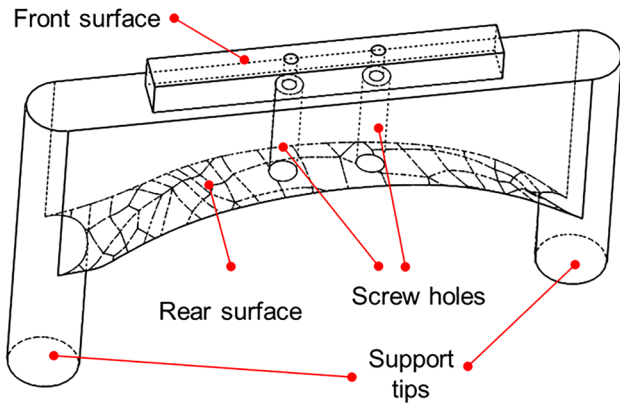


Fig. 3 Initial design of the customized rifle support (*Design 1*)

Table 1 Orthotropic mechanical properties of FDM printed parts using ABS filaments [15]

Printing directions	X	Y	Z
Elastic modulus (GPa)	2.18	2.50	2.26
Tensile strength (MPa)	28.47	33.47	8.39

in Fig. 2b, using Materialise Magics software (Materialise, Belgium). Figure 2c shows a definition of the contact region of the rifle support marked in green, and a customized rifle support was designed using Unigraphics NX8 (Siemens, Germany), as shown in Fig. 2d.

Figure 3 shows the initial design of the customized rifle support (*Design 1*). The rear surface was generated based on the scanned surface of the human body for customization. The front surface was designed as a flat surface that contains two screw holes for assembly with the rifle. Because this customized rifle support fits the human body, it is expected to hold the rifle more stably in the shooting motion than the conventional standard supports in Fig. 1.

2.2 Consideration of Orthotropic Anisotropy

The designed rifle support was fabricated using an FDM type 3D printer (Cubicon Single, Cubicon Inc., Korea). Acrylonitrile butadiene styrene (ABS) filaments of 1.75 mm diameter (Shenzhen ESUN Industrial Co. Ltd., China) were used as printing material. Because an FDM printed part is known to have orthotropic anisotropy, the tensile test specimens were built along X-, Y-, and Z-directions using the current printer and filament. Tensile tests were then performed for the directionally printed specimens, and their results are compared in Table 1 [15]. These orthotropic properties were used in the structural FE analysis and topology optimization.

Because topology optimization is based on FE structural analysis of which results depend on anisotropic material

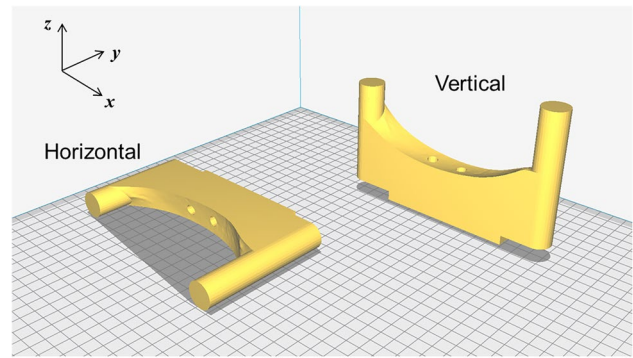


Fig. 4 Description of printing directions (horizontal and vertical printing)

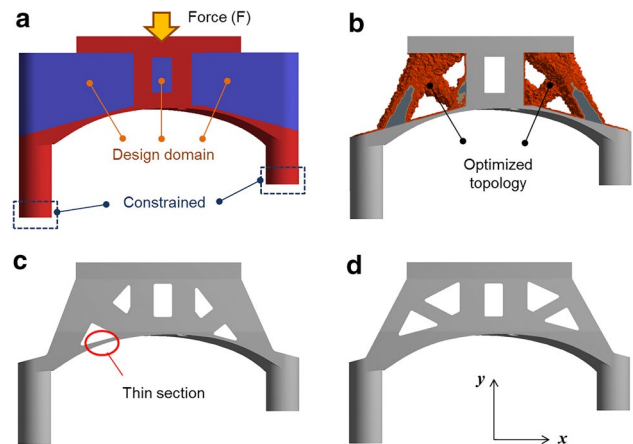


Fig. 5 Topology optimization of the rifle support: a analysis domain and boundary conditions; b optimized topology; c optimized design (*Design 2*); and d reinforced design (*Design 3*)

properties, printing direction should also be determined by considering this orthotropic anisotropy. Two printing directions, horizontal and vertical printing directions, were considered as illustrated in Fig. 4. FE analyses were then performed for these two printing directions because their directional elastic modulus and tensile strength are different according to the printing direction.

2.3 Topology Optimization

Topology optimization was performed based on the initial design. ANSYS Workbench 19.0 (ANSYS Inc., USA) was used to perform a structural FE analysis and topology optimization. Figure 5a shows the analysis domain and boundary conditions for the structural analysis and topology optimization. In this analysis domain, three blue regions were set as the design domain in which some elements will be eliminated selectively. The red regions, including the front and rear ends,

screw holes, and two support tips were excluded from the topology optimization because they should remain.

As boundary conditions for the structural FE analysis, 1 kN force was applied on the front surface along the downward direction, and two support tips were constrained. The objectives of the topology optimization were set to maximize bending stiffness (i.e. compliance minimization) along the vertical direction and to minimize the volume of the design domain. Therefore, the current boundary condition was imposed to evaluate the bending stiffness of the rifle support as an equivalent manner. The related experimental conditions will be explained in Sect. 3.3.

Figure 5b shows the optimized topology in which the design domain volume was reduced to 26% of the original volume. This optimized topology was slightly modified by smoothing its boundary surfaces, as shown in Fig. 5c (*Design 2*). The volume of *Design 2* was 102.2 cm³, which corresponded to 60% of the volume of the initial design (171.6 cm³). However, the optimized result included two thin sections in the rear region of which minimum thickness was 0.84 mm (marked in Fig. 5c).

This design was further modified for structural reinforcement by enhancing the thin section. Figure 5d shows the reinforced design (*Design 3*) in which the minimum thickness of the rear region was increased to 8.34 mm. Instead, quadrilateral holes were enlarged to maintain the total volume (102.1 cm³) similar to *Design 2*. These three designs were then compared through FE analyses, which will be discussed in the next section.

3 Structural Finite Element Analysis

3.1 Comparison of Bending Stiffness

Structural FE analyses were performed for three design cases. The orthotropic elastic modules and boundary conditions were set to be the same as those used in Sect. 2.3. Because the current boundary condition is expected to result in bending deformation, the bending stiffness (k) was defined as follows:

$$k = \frac{F}{\delta_{\max}} \quad (1)$$

where F is the applied force, and δ_{\max} is the maximum vertical (–Y directional) displacement, respectively.

For a relative comparison of the bending stiffness considering volume reduction in the modified geometries, a relative bending stiffness (k^*) was defined as follows:

$$k^* = \frac{V}{V_0} \frac{F}{\delta_{\max}} = \frac{V}{V_0} k \quad (2)$$

where V is the volume of each design and V_0 is the volume of the initial design. Therefore, a higher relative stiffness

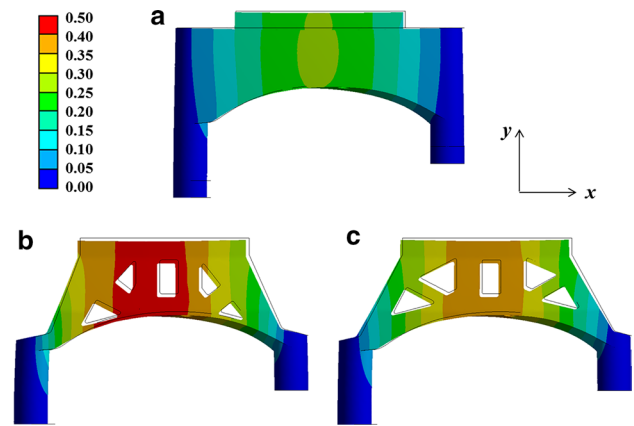


Fig. 6 Comparison of vertical displacements (unit: mm): **a** initial design (*Design 1*), **b** optimized design (*Design 2*), and **c** additionally reinforced design (*Design 3*)

Table 2 Comparison of displacement and stiffness for three designs (horizontal printing case)

Design no.	<i>Design 1</i>	<i>Design 2</i>	<i>Design 3</i>
V (cm ³)	171.6	102.2	102.1
δ_{\max} (mm)	0.258	0.489	0.395
k (N/mm)	3846	2040	2564
k^* (N/mm)	3846	3400	4346

indicates a better stiffness-to-volume ratio, which is the main purpose of weight reduction by topology optimization.

Figure 6a–c show the distributions of the vertical displacements of the three designs for the horizontal printing case. Here, the deformed shapes are magnified by fivefold scale. The resulting deformation and stiffness values are compared in Table 2. It can be seen that the deformation of *Design 2* is twice that of *Design 1* while its volume is 60% of *Design 1*. As a result, the relative stiffness of *Design 2* (3400 N/mm) is lower than that of *Design 1* (3846 N/mm). This undesirable result is due to the thin section of *Design 2*, as marked in Fig. 5c, where displacement was larger than the other region.

On the other hand, the deformation of *Design 3* (0.395 mm) was smaller than that of *Design 2* (0.489 mm). The resulting relative stiffness is 4346 N/mm, which is the highest result among the three cases and corresponds to a 13% improvement from *Design 1*. This indicates that *Design 3* is the most efficient design in terms of stiffness, by reinforcing the thin section and by maintaining a similar topology with the topologically optimized design (*Design 2*).

FE analyses were also performed for the vertical printing case, and their results are given in Table 3. The overall trend that *Design 3* shows the highest relative stiffness (3855 N/mm) was the same as the horizontal printing case. However,

Table 3 Comparison of displacement and stiffness for three designs (vertical printing case)

Design no.	<i>Design 1</i>	<i>Design 2</i>	<i>Design 3</i>
V (cm ³)	171.6	102.2	102.1
δ_{\max} (mm)	0.289	0.527	0.436
k (N/mm)	3460	1898	2294
k^* (N/mm)	3460	3186	3855

this value is lower by 12.7% compared to the horizontal printing case (4346 N/mm), which indicates that the horizontal printing is superior to the vertical printing in terms of the stiffness.

3.2 Comparison of Structural Safety

Figure 7a–c show the equivalent stress distributions of the three designs for the horizontal printing case. In each design, the maximum stress region was marked and the relevant 3-dimensional view was magnified for better understanding. It can be seen that the maximum stress position was the thin section in *Design 2* whereas these positions were near lower holes for the other cases. This indicates that the thin section in *Design 2* should be reinforced from the viewpoint of structural safety as well as stiffness.

To discuss structural safety of the lightweight rifle support, the safety factor (λ) was considered by taking the relative ratio of the allowable stress (σ_{allow}) to the maximum equivalent stress (σ_{max}). The relative safety factor (λ^*) was then defined by multiplying the volume ratio to the safety factor, as the following equation:

$$\lambda^* = \frac{V}{V_0} \frac{\sigma_{\text{allow}}}{\sigma_{\text{max}}} = \frac{V}{V_0} \lambda \tag{3}$$

where the allowable stress was set to directional tensile strength in Table 1. Because it is known that a 3D-printed ABS part shows brittle behavior along the thickness direction [16], the maximum normal (Z-directional) stress was taken as the maximum stress along the thickness direction while the equivalent stress was taken for in-plane maximum stress to describe the ductile behavior along the in-plane direction.

Table 4 compares the resulting structural safety of three designs for the horizontal printing case. The maximum stresses and relative safety factors were compared both along the in-plane and thickness directions. It can be seen that *Design 3* shows the highest relative safety factors in both directions, showing improvements of 23–43% according to the printing direction. This indicates that *Design 3* is the most efficient design in terms of the structural safety as well as the bending stiffness.

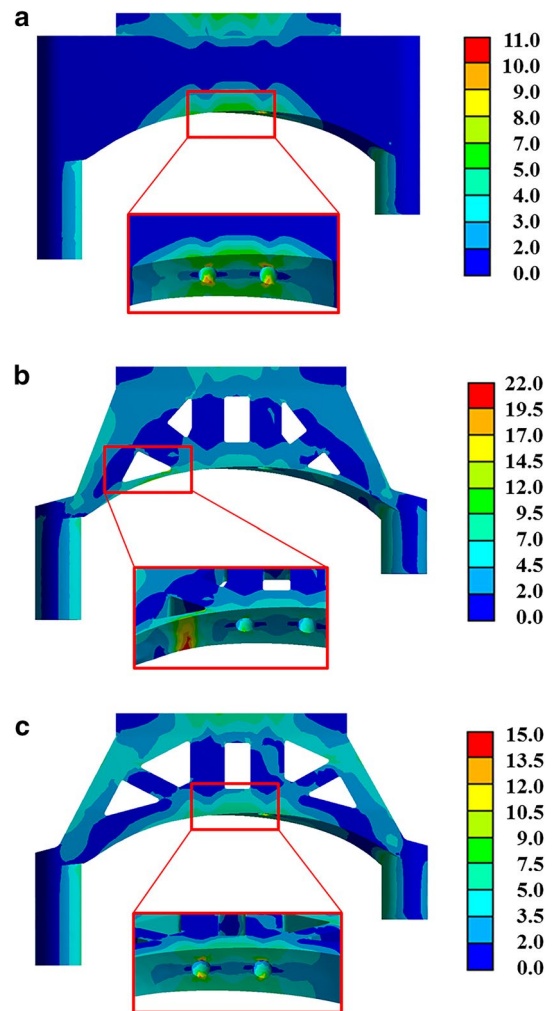


Fig. 7 Comparison of equivalent stress (unit: MPa): **a** initial design (*Design 1*), **b** optimized design (*Design 2*), and **c** reinforced design (*Design 3*)

Table 4 Comparison of structural safety for three designs (horizontal printing case)

Design no.	<i>Design 1</i>	<i>Design 2</i>	<i>Design 3</i>
σ_{max} (MPa)			
In-plane	10.90	22.02	14.87
Thickness	3.64	5.03	4.29
λ^*			
In-plane	2.61	2.17	3.21
Thickness	2.30	2.80	3.29

The results for the vertical printing case are given in Table 5, which also reveals that *Design 3* shows the highest safety factors along both in-plane and thickness directions. The relative safety factor along the in-plane direction (3.36) was higher than that of the horizontal printing case (3.21).

Table 5 Comparison of structural safety for three designs (vertical printing case)

Design no.	<i>Design 1</i>	<i>Design 2</i>	<i>Design 3</i>
σ_{max} (MPa)			
In-plane	10.57	21.17	14.24
Thickness	4.13	4.98	4.30
λ^*			
In-plane	2.69	2.26	3.36
Thickness	2.03	2.83	3.28

On the other hand, the relative safety factor along the thickness direction (3.28) was slightly lower than that of the horizontal printing case (3.29). However, these differences are less significant than the difference of the relative stiffness as mentioned in Sect. 3.1 (12.7%). As a consequence, *Design 3* was selected as the optimal design, and the horizontal direction was selected as the desirable printing direction.

3.3 Experimental Verification

The final design of the customized rifle support (*Design 3*) was then printed using the FDM type 3D printer. The initial design without topology optimization (*Design 1*) was also printed for comparison. The printing direction was set to the horizontal direction for both cases, and the layer thickness was set to 0.2 mm. The nozzle temperature, bed temperature, and feed rate were set to 240 °C, 115 °C, and 200 mm/s, respectively.

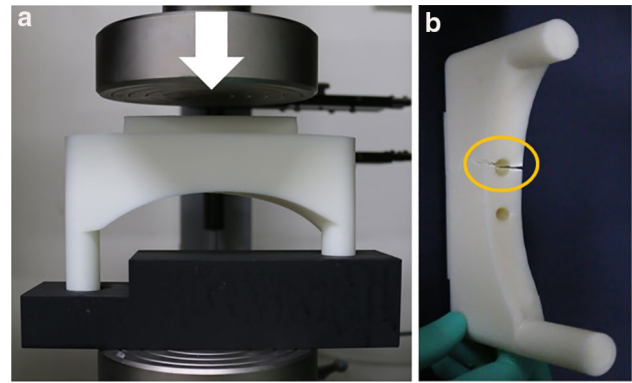
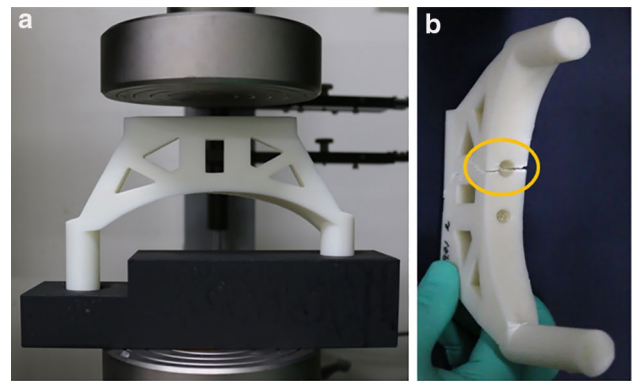
Compression tests were then performed to evaluate the structural safety of the printed rifle supports. Compression tests were performed using a universal test machine (NA-2M, Nanotech, Korea) with a compression speed of 1 mm/min. These tests were continued until failure occurred, and the critical force at failure (F_{crit}) was measured for each case. Five experiments were performed for each design.

To consider the weight reduction effect of the optimized topology, the relative critical force (F^*) was defined by dividing the critical force by its weight, as given in the following equation [17]:

$$F^* = \frac{1}{mg} F_{crit} \quad (4)$$

where m is the mass of each printed support and g is the acceleration of gravity (9.81 N/m²). Therefore, the relative critical force (F^*) means the ratio of endurable load of a rifle support with respect to its weight.

Figure 8a shows the experimental setup for the compression test of *Design 1*, and the resulting failure location is shown in Fig. 8b. It can be seen that the failure location is identical with the maximum stress positions in Fig. 7a. Figure 9a, b show the experimental setup and the resulting

**Fig. 8** Compression test of the rifle support for the initial design (*Design 1*): **a** experimental setup, **b** failure location**Fig. 9** Compression test of the rifle support for the final design (*Design 3*): **a** experimental setup, **b** failure location**Table 6** Comparison of the compression test results

Design no.	<i>Design 1</i>	<i>Design 3</i>
m (g)	168.2 ± 0.27	99.4 ± 0.08
F_{crit} (kN)	16.84 ± 0.52	13.92 ± 0.22
F^*	10,194 ± 321	14,294 ± 225

failure location for *Design 3*, respectively. The failure location is also the similar to the simulation result in Fig. 7c, which indicates that the FE analyses of the 3D-printed rifle supports considering the orthotropic material property provides reliable estimation of failures.

Table 6 compares the compression test results quantitatively, including mass information for each design. The critical forces were measured to be 16.84 kN for *Design 1* and 13.92 kN for *Design 3*. The relative critical force (F^*) for *Design 3* was calculated to be 14,294, which indicates the current design can endure 14000 times heavier load than its own weight. This result corresponds to a 40% improvement compared with that of the initial design (10,194), showing

good agreement with the FE analysis results in Table 4. Therefore, it can be concluded that the proposed design with optimized topology provides an efficient structure in terms of stiffness and safety.

4 Conclusions

In this study, a customized rifle support for biathlon was developed to maintain stable shooting motion. 3D scanning was performed to obtain the geometry of an athlete's body, and a rifle support was designed to fit the athlete's body (*Design 1*). Topology optimization combined with a FE analysis was then performed to reduce the part weight as well as to ensure allowable structural safety and stiffness. In the FE analyses and topology optimization, orthotropic material anisotropy was considered and the relevant effect of printing direction was taken into account. Because the topologically optimized design (*Design 2*) contained a locally thin structure where stress was concentrated, additional structural reinforcement was conducted (*Design 3*), which shows further improvement in structural stiffness and safety. The final design and printing direction were then selected as *Design 3* and horizontal direction, respectively. The FE analysis result for the final design and printing direction showed improvements in the specific stiffness (by 12.7%) and in the relative structural safety (by 23–43%, according to the direction).

The final design was fabricated using an FDM type 3D printer, and its structural safety was evaluated by compression tests. It was found that the printed rifle support could endure 13.92 kN load, which corresponded to 14,294 times its weight (99.4 g). This result corresponds to 40% improvement from its original design (10,194), which indicates that the proposed design based on topology optimization is superior to its original design. Considering that the printed rifle support weighs less than 100 g, it can be utilized in real biathlon competition without a significant increase in the rifle weight.

Acknowledgements This study was supported by a grant from the Technology Innovation Program (Grant no: 10062348) funded by the Ministry of Trade, Industry & Energy (MOTIE, Korea) and by a grant from the National Research Foundation of Korea (NRF) funded by the Ministry of Science and ICT (Grant number: NRF-201902799).

References

- Kim, Y. H., & Han, S. Y. (2017). Topological shape optimization scheme based on the artificial bee colony algorithm. *International Journal of Precision Engineering and Manufacturing*, 18(10), 1393–1401.
- Rozvany, G. I. (2009). A critical review of established methods of structural topology optimization. *Structural and Multidisciplinary Optimization*, 37(3), 217–237.
- Zegard, T., & Paulino, G. H. (2016). Bridging topology optimization and additive manufacturing. *Structural and Multidisciplinary Optimization*, 53(1), 175–192.
- Dewhurst, P., & Srithongchai, S. (2005). An investigation of minimum-weight dual-material symmetrically loaded wheels and torsion arms. *Journal of Applied Mechanics*, 72(2), 196–202.
- Rezaie, R., Badrossamay, M., Ghaie, A., & Moosavi, H. (2013). Topology optimization for fused deposition modeling process. *Procedia CIRP*, 6, 521–526.
- Gaynor, A., Meisel, N., Williams, C., & Guest, J. (2014). Multiple-material topology optimization of compliant mechanisms created via PolyJet three-dimensional printing. *Journal of Manufacturing Science and Engineering*, 136(6), 061015.
- Jang, S., Goh, C. H., & Choi, H. J. (2015). Multiphase design exploration method for lightweight structural design: Example of vehicle mounted antenna-supporting structure. *International Journal of Precision Engineering and Manufacturing-Green Technology*, 2(3), 281–287.
- Kotlinski, J. (2014). Mechanical properties of commercial rapid prototyping materials. *Rapid Prototyping Journal*, 20(6), 499–510.
- Kok, Y., Tan, X. P., Wang, P., Nai, M. L. S., Loh, N. H., Liu, E., et al. (2018). Anisotropy and heterogeneity of microstructure and mechanical properties in metal additive manufacturing: A critical review. *Materials and Design*, 139(5), 565–586.
- Ho, C. M. B., Ng, S. H., & Yoon, Y. J. (2015). A review on 3D printed bioimplants. *International Journal of Precision Engineering and Manufacturing*, 16(5), 1035–1046.
- Chen, R. K., Jin, Y. A., Wensman, J., & Shih, A. (2016). Additive manufacturing of custom orthoses and prostheses—A review. *Additive Manufacturing*, 12, 77–89.
- Kim, Y. K., & Joo, J. Y. (2017). Effects of custom-made 3D printed insoles for flat feet people on gait parameters. In *Proceedings on 35th conference international society biomechanical sports, Cologne, Germany* (pp. 195–198).
- Hoffman, M. D., Gilson, P. M., Westenburg, T. M., & Spencer, W. A. (1992). Biathlon shooting performance after exercise of different intensities. *International Journal of Sports Medicine*, 13, 270–273.
- Baca, A., & Kornfeind, P. (2012). Stability analysis of motion patterns in biathlon shooting. *Human Movement Science*, 31(2), 295–302.
- Lim, Y. E., Kim, N. H., Choi, H. J., & Park, K. (2017). Design for additive manufacturing of customized casts with porous shell structures. *Journal of Mechanical Science and Technology*, 31(11), 5477–5483.
- Tam, K. M. M., & Mueller, C. T. (2017). Additive manufacturing along principal stress lines. *3D Printing and Additive Manufacturing*, 4(2), 63–81.
- Lim, Y. E., Park, J. H., & Park, K. (2018). Automatic design of 3D conformal lightweight structures based on a tetrahedral mesh. *International Journal of Precision Engineering and Manufacturing-Green Technology*, 5(4), 53–60.

Publisher's Note Springer Nature remains neutral with regard to jurisdictional claims in published maps and institutional affiliations.



Jung-Hwan Park received his B.S. degree in Mechanical System Design Engineering at Seoul National University of Science and Technology, Korea, in 2017. He is currently a master candidate in the Department of Mechanical Design and Robot Engineering at National University of Science and Technology. His research interest is design and additive manufacturing of lightweight structures based on topology optimization and micro-lattice structures.



Bona Goo received her B.S. degree in Mechanical System Design Engineering at Seoul National University of Science and Technology, Korea, in 2018. She is currently a master candidate in the Department of Mechanical Design and Robot Engineering at Seoul National University of Science and Technology. Her current research interests include 4D printing and additive manufacturing of lightweight structures.



Keun Park received his B.S. and M.S. degrees in Precision Engineering and Mechatronics at KAIST, Korea, in 1992 and 1994, respectively. He then received his Ph.D. degree in Mechanical Engineering from KAIST in 1999. Dr. Park is currently a Professor of the Department of Mechanical System Design Engineering at Seoul National University of Science and Technology, Korea. His research interests include numerical analysis of material forming processes, micro-fabrication, and

additive manufacturing.